Journal of Avian Medicine and Surgery 40(1):56–66, 2026

Original Study

Musculoskeletal Ultrasonography in Normal Feral Pigeons (*Columba livia* F. *dom.*)

Anna Korshunova, Volker Schmidt, Susan Orosz, Holger Kirsten, and Maria-Elisabeth Krautwald-Junghanns

Abstract: Avian orthopedic disorders are common but can be challenging to diagnose. Radiographic examination and, to a lesser extent, computed tomography are the main diagnostic techniques used to assess avian orthopedic problems, whereas sonography is rarely applied. The objective of this study was to determine whether B-mode ultrasonography could be used to noninvasively evaluate the pectoral region and peripheral skeleton of 17 live feral pigeons (*Columba livia* f. dom.) (body weight: 270 ± 34.5 g) presented for clinical examination. The ultrasound examination (General Electric ≥ LOGIQ S7 Expert, GE Healthcare, Buckinghamshire, UK) was performed using a GE L8-18I-D "hockey stick" transducer with an 8–18 MHz frequency range (AME Ultrasound, Suffern, NY, USA). The results of the pigeon ultrasound examinations provided clinical data regarding the bone cortex and surrounding soft tissues of the pectoral region, shoulder girdle, wing, and leg. The overall long bone thickness, total cortical bone thickness, and clavicle thickness of each bird were measured using radiography and B-mode sonography to determine the statistical concordance between these diagnostic methods using the Lin concordance correlation coefficient and Bland-Altman plots. Fisher z-transformation was used to calculate 95% confidence intervals and standardize *P* values for each connection. The agreement analysis revealed a significant positive concordance between radiographic and ultrasound measurements for overall long bone thickness (Lin concordance correlation coefficient = 0.655, 95% CI: 0.520-0.758, $P < 0.001$); no other comparisons were significant. This study provides evidence that B-mode ultrasonography can qualitatively assess pigeons' musculoskeletal systems, notably in the pectoral area and proximal limbs. This technique can also be used to acquire measurements of the structures thicker than 0.2 cm, which may be used for osteosynthesis planning or monitoring neoplastic conditions posttreatment.

Key words: orthopedics, musculoskeletal system, diagnostic imaging, ultrasonography, avian medicine, feral pigeon, *Columba livia f. dom*

INTRODUCTION

Orthopedic problems are prevalent in avian medicine with trauma-related fractures and dislocations being the most common musculoskeletal conditions affecting free-ranging birds.[1] Additional orthopedic issues documented in avian patients include degenerative joint diseases, metabolic abnormalities, arthritis, soft tissue injuries, and circulatory disorders.[1] The early identification of medical problems can have a positive influence on the overall prognosis for avian patients. Rapid diagnosis and assessment are extremely helpful, especially for injured birds that are presented to wildlife hospitals. For wildlife patients, the duration and approach of treatment and management influence the rehabilitation outcome of each case. Therefore, an effective, less invasive diagnostic imaging modality would be of benefit to veterinarians treating avian orthopedic problems and injuries.

Feral pigeons (*Columba livia* f. dom.) are common urban wildlife and are often diagnosed with musculoskeletal disorders.[2] These injuries include traumatic encounters with urban infrastructure, predation, or human intervention (eg, illegal hunting).[2–8]

Avian veterinarians often use radiography as a primary diagnostic technique. This approach demonstrates the highest efficacy for fracture diagnoses and preliminary

From the Clinic for Birds and Reptiles, University of Leipzig, An den Tierkliniken 17, 04103, Leipzig, Germany (Korshunova, Schmidt, Krautwald-Junghanns); the Bird and Exotic Pet Wellness Center, 5166 Monroe Street, Suite 306, Toledo, OH 43623, USA (Orosz); and the Institute of Medical Informatics, Statistic and Epidemiology, University of Leipzig, Haertelstrasse 1, 04107, Leipzig, Germany (Kirsten); †, Krautwald-Junghanns, deceased.

Corresponding Author: Anna Korshunova, anna.a.korshunova@gmail.com

diagnostic evaluation. Radiographic imaging offers critical insights into bone structure and often provides a comprehensive review of the bird's entire body.[9–12] However, the diagnostic quality of a single-plane radiographic view may be restricted in certain cases due to the summation of anatomical features. As a result of the overlap of bony structures, including the clavicle (*os clavicula*), coracoid (*os coracoideum*), and scapula (*os scapula*), radiographic evaluation of the avian shoulder girdle with conventional diagnostic planes can be particularly difficult. To better assess these patients, the supplemental radiographic plane (H-view) may be helpful in enhancing the visualization of shoulder girdle structures.[13] Moreover, exterior soft tissues undergo limited radiographic assessment, thus restricting the diagnostic capabilities of this approach regarding the avian musculoskeletal system.[9,11]

Computed tomography (CT) has become a more accessible diagnostic imaging modality in exotic medicine. It can provide useful diagnostic information regarding soft tissue structures while avoiding superimposition artifacts.[9,10] However, CT imaging is associated with high material costs for the veterinary hospital and bird owner.[11]

Ultrasonography (US) is a cost-effective, noninvasive, real-time diagnostic modality whose diagnostic value and capabilities have been described and used in avian patients for decades, primarily in examining internal and visual organs.[9,11,14] B-mode US for assessing bones and soft tissues (eg, muscles, ligaments, nerves), joint cavities, and blood vessels has been described in humans and mammals, including dogs, horses, and laboratory animals.[15–21] Several studies described the use of US to diagnose bone tissue diseases, such as fractures in children and osteomyelitis and osteochondrosis in small mammals.[11] Ultrasound has also been reported as a viable diagnostic imaging modality to assess soft tissue swellings, muscles, tendons, and joints in exotic animals.[9,11] The use of color and power Doppler US is valuable for evaluating blood flow in specific organs or lesions, ischemia, or the extent of vascularization of a tissue mass.[11] However, the potential application of US in avian orthopedics is currently limited to a few studies. González et al[14] described using B-mode US to assess long bones on cadavers of several *Strigiformes* and *Accipitriformes* species. Additionally, the González et al[14] investigation provided information on the effectiveness of B-mode US for fracture assessment in live avian patients and a clinical example of the real-time sonography monitoring of manual approximation and surgical fixation of bone fragments in a barn owl (*Tyto furcata*).

The hypotheses for this study were that B-mode ultrasonography could be used to provide supplementary diagnostic information to radiography by enabling subjective assessment of periosteal surfaces and surrounding soft tissues, and that measurements of overall long bone thickness obtained using ultrasonography would demonstrate significant concordance with radiographic measurements, whereas thinner cortical structures might show lower or non-significant concordance. Using qualitative data and descriptions of intact structures in live feral pigeons, our results describe the basic concepts of musculoskeletal B-mode US that may be used on avian patients.

MATERIALS AND METHODS

Animals

This study included 17 adult feral pigeons that were presented for examination at the Clinic for Birds and Reptiles of the University of Leipzig (Leipzig, Germany) between March 2022 and January 2024 with various clinical signs due to suspected trauma or other musculoskeletal disorders. The birds had body condition scores between 2 and 3 out of 5, determined by the degree of pectoral muscle prominence on a 5-point scale: 1 (emaciated), 2 (lean), 3 (well-conditioned), 4 (overconditioned), and 5 (obese). Sex determination within the clinical and nontarget visual studies was limited. The absence of polyostotic hyperostosis, active gonads, or calcified eggs determined through interpretation of radiographic images provided evidence that all birds included in the study were apparently sexually inactive. Following clinical inspection and radiographic imaging, all pigeons were examined by B-mode US and showed no abnormalities of the musculoskeletal system.

Samples

The study was designed to qualitatively and statistically evaluate radiographic and US assessment of the images obtained, where radiography is currently the preferred approach. For radiographic imaging, birds were fully conscious and manually restrained to an acrylic plate. Radiographic images were obtained in both lateral and ventrodorsal views with a commercial digital Gierth HF200 radiographic unit (Gierth X-Ray International GmbH, Riese, Germany). Birds were held in dorsal recumbency with their legs retracted caudally and their wings extended laterally for ventrodorsal positioning. The positioning of the bird in the ventrodorsal radiographic view was considered sufficient if the sternum was superimposed on the spine and the wings were symmetrical. For the lateral view, birds were restrained

in right lateral recumbency with their wings stretched posteriorly and their legs extended and overlapped to reduce summation. The radiographic images were evaluated and the total bone thickness measurements of the clavicle, humerus, ulna, radius, femur, and tibia, together with the cortical bone thickness of these bones, were conducted using the Fujifilm Console Advance Program (Jakarta Selatan, Indonesia). Each anatomical measure was assessed in the mid-diaphyseal region of the bones 3 times with the averages of the measurements documented.

Musculoskeletal US was conducted using a sonography device (General Electric LOGIQ S7 Expert, GE Healthcare, Buckinghamshire, UK) with an 8–18 MHz frequency GE L8-18I-D "hockey stick" transducer (AME Ultrasound, Suffern, NY, USA) to access shallow tissue depth. The veterinary assistant restrained the conscious birds vertically with a handling method in which the bird's head was controlled between the thumb and the index finger, the bird's legs were restrained with the index and ring fingers of the other hand by having the middle finger between the legs to avoid iatrogenic damage, and the rest of the fingers of the lower hand controlled the wings tips.[22,23] The region of interest (ROI) was cleaned, feathers were clipped, and ultrasound gel (Aquasonic Ultrasound Gel, Fairfield, NJ, USA) was applied before each examination. Each US examination was conducted by a single sonography expert (AK), and the procedures were typically performed within 3–5 minutes. The following ROI were examined: pectoral region (sternum, pectoral muscle), shoulder girdle (coracoid, clavicle scapula, shoulder joint including *ligamentum acrocoracohumeralis*), humerus, elbow joint, radius, ulna, carpometacarpal joint, carpometacarpus, coxofemoral joint, femur, stifle joint, tibiotarsus, intertarsal joint, and tarsometatarsus. We applied short- and long-axis US images for most of the assessed ROI. The thickness measurements of the sternum (*os sternum*), pectoral muscle (*m. pectoralis superficialis et profundus*), coracoid (*os coracoideum*), clavicle (*os clavicula*), *lig. acrocoracohumeralis*, humerus (*os humerus*), ulna (*ulna*), radius (*radius*), and femur (*os femoris*) bones and the cortical bone thickness of these bones were assessed by placing the US transducer perpendicular to the long axis of the anatomical structure and by using the measurement tool on the US device. Each anatomical measure was assessed in the mid-diaphyseal region 3 times, and the means of the measurements were recorded. Short-axis thickness in 3 anatomical sections (cranial, medial, and caudal) was measured on the pectoral muscle (*m. pectoralis*). Cortex thickness was measured in 3 anatomical sections (cranial, medial, and caudal) in pectoral bone; short-axis bone thickness was measured in shoulder girdle bones (coracoid, clavicle, scapula). Cross-bone thickness in 2 axes (long- and short-axis) and cortical thickness in the short-axis were measured in the humerus, ulna, radius, femur, and tibiotarsus. The cross-sectional thickness of the long bones—humerus, ulna, radius, femur, and tibiotarsus—along with the overall cortical bone thickness of the evaluated long bones and clavicle thickness, measured along the short-axis, were compared with the radiographic assessment of the same ROI using the Lin concordance correlation coefficient (CCC). The transverse thickness of the acrocoracohumeral ligament (*lig. acrocoracohumeralis*) at the dorsal tubercle of the humerus was measured in a single dimension within the shoulder joint.

Data analysis

Based on the quality of the visual image, we created a grading system for ROI accessibility (good, moderate, and poor). The grading scale was based on a subjective assessment of image clarity and the feasibility of accurate measurement evaluation: good (the image is clear, and the obtained structure is well-defined and measurable), moderate (the acquired structure is insufficiently defined), and poor (the acquired structure is nearly indefinable, unable to obtain measurements). Lin CCC was calculated to measure agreement between radiographic and US measurements for 3 groups: overall long bone thickness, total cortical bone thickness, and clavicle thickness using the DescTools package (Signorell, 2025).[24] For each correlation, 95% confidence intervals were computed using Fisher z-transformation, and P values were derived by standardizing the z-transformed correlation coefficients. For linear regression, the normality of residuals was verified using the Shapiro-Wilk test for the significant correlation to ensure validity. Both scatterplots for CCC and Bland-Altman plots were created using the software R-Project (R package, version 0.99.60, Helsana Versicherungen AG, Health Sciences, Zurich, Switzerland).

RESULTS

During the study, 520 sonographic images were obtained. At least 2 images were obtained for each ROI, and these were assessed according to the established image quality evaluation scale (Table 1). The obtained measurements of the selected anatomical regions are shown in Table 2. The agreement analysis revealed significant concordance between radiographic and US measurements for the overall long bones thickness (Lin CCC = 0.655, 95% CI: 0.520–0.758, $P < 0.001$) (Fig 1). The Shapiro-Wilk test on residuals

indicated no significant departure from normality ($P = 0.42$). Based on linear regression analysis, the formula to convert US measurements to radiographic equivalents is radiographic image $= 0.1161 + 0.6227 \times$ US with US providing approximately 46% of the variability of the radiographic data. In contrast, total cortical bone thickness (0.06 ± 0.068 cm) and clavicle thickness (0.096 ± 0.024 cm) showed no agreement between US and radiographic measurements (Lin CCC $= 0.011$, 95% CI: -0.061 to 0.084, $P > 0.05$ and 0.108, 95% CI: -0.142 to 0.346, $P > 0.05$, respectively), indicating no data concordance (Fig 1). For the overall long bone thickness, the Bland-Altman plot demonstrated minimal systematic bias with limits of agreement (mean $\pm$ 2 SD) indicating acceptable measurement precision.

Ultrasound results

Sonographic imaging of the pectoral region: Image accessibility was highest in the pectoral musculature and sternum. These anatomical structures were accessed using ventral long- and short-axis US views. The US transducer was placed directly on the pectoral apteria region in 3 dimensions (at the cranial, middle, and caudal third) (Fig 2). In the ventral short-axis view, a slice of the superficial and deep pectoral muscles, delimited by a fascial layer in the form of a hyperechoic line, was obtained. The sternum was visualized as an L-shape hyperechoic line, not allowing US waves to pass. This made it possible to observe the reverberation lines in the deeper tissues. The US scan of the muscle tissue showed a regular, isoechoic, nonhomogeneous pattern. The ventral long-axis view showed no discernible difference between the superficial and deep pectoral muscle divisions. As a result of the muscle tissue reflecting off the surface of the sternum in the ventral long-axis view, a mirror effect may appear, repeating in the lower portion of the image.

Sonographic imaging of shoulder region: The bones of the shoulder girdle (clavicle, coracoid, scapula) showed slightly lower accessibility, which might occur due to the superficial location of the bony structures and the lack of soft tissue, which acts as a conductor of the US beam between the transducer and the examination area. Nevertheless, the quality of the images was sufficient to assess the bone integrity over almost the entire length. The craniolateral long-axis view was used to display and obtain the thickness measurements of the coracoid and clavicular bones (Fig 3.1). Both appeared to have medium echogenicity with hyperechoic cortical layers on both sides. Due to the dense bone tissue's acoustic shadow, only the coracoid bone's dorsal surface could be occasionally observed in birds weighing more than 300 g. The comparative measurements of the clavicle were obtained on the ventrodorsal radiographic views. To access the scapula in long- and short-axes on the dorsal views, the transducer was placed on the dorsal side of the thorax. The scapula was more difficult to visualize, likely due to the complex structure of the hook-shaped acrocoracoid process (*processus acrocoracoideus*) and the lack of soft tissue coverage.

Radiographic measurements of the coracoid and scapula thickness were not performed because the views used in this study did not allow visualization of this area in the same plane as obtained by sonography.

Table 1. Sonographic approaches and their assessment quality ranking in the examined anatomical regions in feral pigeon (*Columba livia* f. dom.).

ROI	View	Assessment quality
Thorax		
Pectoral muscle (m. pectoralis superficialis et profundus)	VT	G
		G
		G
Sternum	VT	G
		G
		G
Shoulder girdle		
Clavicle	CrL	G
Coracoid	CrL	G
Scapula	DT, DL	M
Shoulder joint		
Ligamentum acrocoracoideus	VMT	G
Humerus head	VMT, VML	G
Humerus	VT	G
		G
Elbow joint	VT	P
Ulna	VT	G
Radius	VT	G
Carpal joint	VT	P
Metacarpus	VT	M
Coxofemoral joint	DLT	P
Femur	CdLT	G
		G
		G
Stifle joint	CrT	M
Tibiotarsus		
Tibiotarsus	CrT	G
		G
		G
Fibula	CrT	M
Intertarsal joint	CdL	M
Tarsometastarsus	CrT	P

Abbreviations: ROI, region of interest; VT, ventral transversal; CrT, cranial transversal; CrL, cranial longitudinal; DT, dorsal transversal; DL, dorsal longitudinal; VMT, ventromedial transversal; VML, ventromedial longitudinal; DLT, dorsolateral transversal; CdLT, caudolateral transversal; G, good; M, moderate; P, poor.

Table 2. Mean ± SD (mm) values of sonographic and radiographic measurements of specific musculoskeletal components in feral pigeons (*Columba livia* f. dom., n = 17).

ROI	Parameter	Mean ± SD, mm	
		US	Radiograph
Clavicle	Longitudinal thickness	0.09 ± 0.01	0.08 ± 0.02
Humerus	Cortical bone thickness	0.06 ± 0.02	0.04 ± 0.008
	Medial bone thickness	0.40 ± 0.12	0.43 ± 0.03
Ulna	Cortical bone thickness	0.06 ± 0.01	0.04 ± 0.009
	Medial bone thickness	0.38 ± 0.05	0.37 ± 0.02
Radius	Cortical bone thickness	0.06 ± 0.01	0.03 ± 0.007
	Medial bone thickness	0.26 ± 0.03	0.23 ± 0.008
Femur	Cortical bone thickness	0.06 ± 0.02	0.04 ± 0.006
	Medial bone thickness	0.38 ± 0.05	0.35 ± 0.04
Tibiotarsus	Cortical bone thickness	0.06 ± 0.01	0.04 ± 0.009
	Medial bone thickness	0.35 ± 0.05	0.32 ± 0.05
Total cortical thickness		0.06 ± 0.01	0.04 ± 0.009
Total medial long bones thickness		0.36 ± 0.08	0.34 ± 0.07

Abbreviations: ROI, region of interest; SD, standard deviation; US, ultrasound.

Furthermore, the assessment of the scapula was limited due to the summation in both radiographic views.

The cranio-ventromedial short-axis view allowed the assessment of the shoulder joint (Fig 3.2). The acrocoracohumeral ligament (*lig. acrocoracohumeralis*) was superimposed on the surface of the humeral head as a hyperechoic arch. The ligament could be observed as a "thin hummingbird beak" shape with a parallel fibrillary structure, slightly less echogenic than the bone surface. The thickness of the ligament was also measured on the middle ligaments' length in the sulcus transversus region. *Musculus supracoracoideus* tissue, which courses through the triosseal canal (*canalis triosseus*), was identified in the image's middle section between the ligament and the articular surface.

Sonographic imaging of the wing: Ventral longitudinal and ventral transversal views were used to image the humerus (Fig 4.1), radius, and ulna (Fig 4.2). The antebrachium allowed for better image accessibility. The bony structures on the long-axis approach appeared as hyperechoic lines casting acoustic shadows upon the underlying structures. All long bones appear in the transverse view as irregularly shaped circles, containing a hyperechoic cortical layer and a hypoechoic medullary bone canal region. The transverse ultrasound view assessed the cross-sectional thickness of the wing's bones along the long- and short-axis. Comparative measurements were conducted on radiographic images in both ventrodorsal and laterolateral views at the mid-diaphyseal region, which were compared with the values evaluated along the *y*-axis. Imaging of the humerus, particularly in the short-axis view, can be difficult due to the uneven distribution of adjacent muscle tissue and the pneumatized medullary bone canal. Informative imaging of the elbow and carpal joints was practically impossible due to the nearly complete absence of muscular tissue and the irregular surface of the bony structures.

Sonographic imaging of hip joint: A dorsocaudolateral cross-sectional view was applied to image the hip joint. The US image showed the cranial scapus pubis and trochanter femoral as hyperechoic, regularly formed, barely visible structures, which were nondiagnostic. *Ligamentum ischiofemoralis* and *lig. pubofemoralis* were hard to visualize due to the lack of soft tissues between the sonographic probe and bone surface. However, the joint cavity could be accessed and observed as a hypoechoic, homogeneous area. Sonographic imaging was only possible in the regions of the hip's iliac wing and femoral crest.

Sonographic imaging of the leg: The femur demonstrated good accessibility. The caudolateral long-axis, caudolateral, and lateral short-axis approaches were used (Fig 5.1). In the longitudinal view, the proximal surface of the femur was visible and could be observed as a hyperechoic line. In the transverse view, the entire section of the bone was visible. The central medullary cavity was uniformly hypoechoic, and the cortex was visible as a hyperechoic circle from all sides of the bone (Fig 5.1). Similarly, we used lateral and craniolateral long-axis and lateral short-axis views to examine the tibiotarsus. The longitudinal view allowed visualization of the cortical layer of the tibiotarsus, which was close to the US probe. The fibula could not be identified in the lateral view. In cross-section, the tibiotarsus

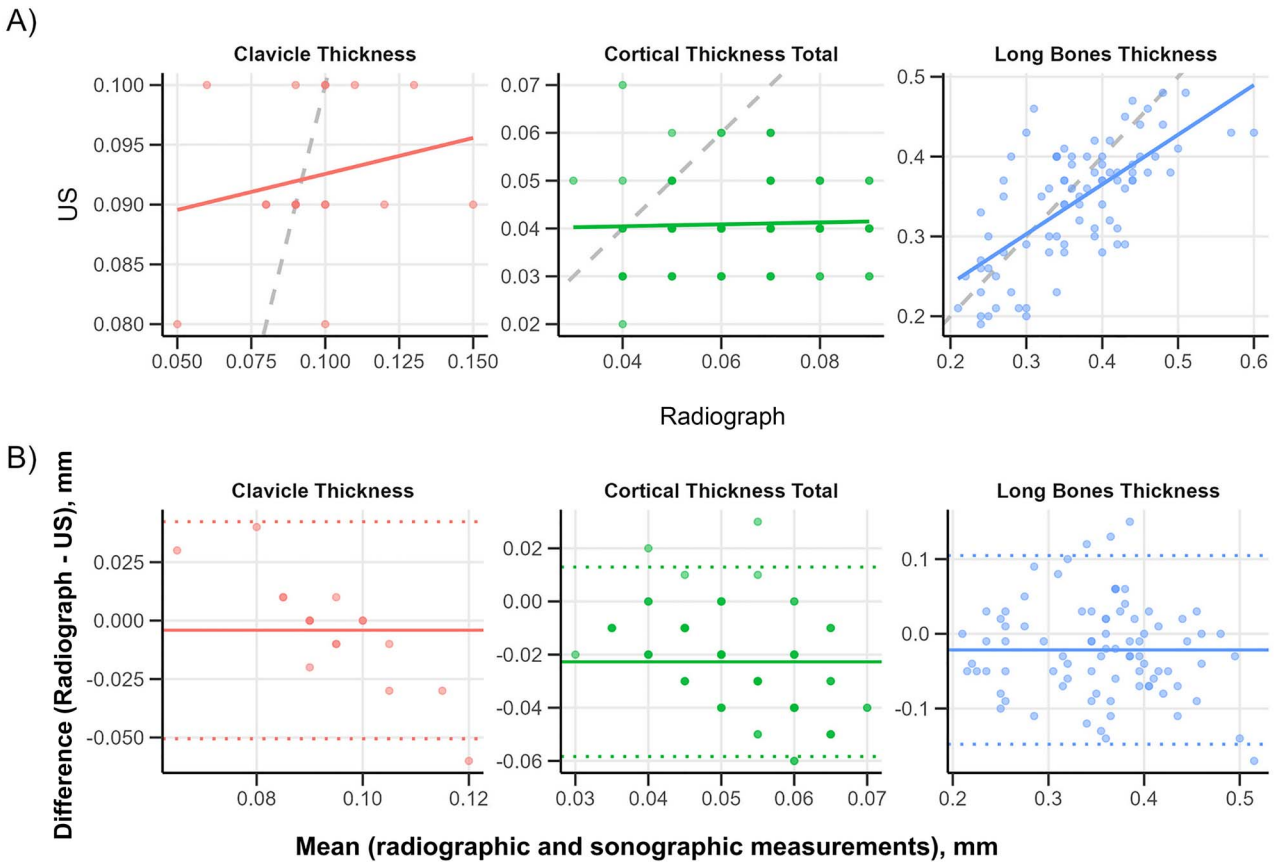

Figure 1. Agreement analysis between radiographic and ultrasound (US) measurements of bone parameters in feral pigeons (*Columba livia* f. dom.) showing the difference and mean value of the radiographic and ultrasonographic measurements (mm). (A) Scatterplots comparing radiographic (*x*-axis) and US (*y*-axis) measurements for clavicle thickness, cortical thickness total, and long bone thickness. Solid colored lines represent linear regression fits for each parameter, whereas dashed gray diagonal lines indicate the line of equality ($y = x$). The deviation between regression lines and the equality line illustrates systematic bias between measurement techniques. (B) Bland-Altman plots displaying the difference between methods (radiographic - US) against their mean with limits of agreement (mean ± 2 SD, dotted lines) and mean bias (solid lines). Correlation between methods was nonstatistically significant for clavicle thickness and total cortical thickness and stronger than expected by chance for long bone thickness (Lin concordance correlation coefficient = 0.655, 95% CI: 0.520-0.758, $P < 0.001$, n = 85).

appeared as an irregularly shaped circle with a hyperechoic cortical layer and a hypoechoic medullary canal. The fibula had increased visual clarity in the craniolateral short-axis view, where it was observed to have a hyperechoic oval structure (Fig 5.2). The cross-sectional thickness of the femur and tibiotarsus was measured in the same manner as the wing. The stifle joint was examined with the tibiotarsus flexed at 90° and showed poor assessment on average. The medial and lateral condyles of the femur and the articular surface of the tibia could be visualized. The tarsal and tarsometatarsal joints were inaccessible due to the lack of soft tissue and the dense horn covering the distal pelvic limb. Comparative radiographic measures of the femur and tibiotarsus were acquired using the lateral view. The comparative radiography evaluation of the stifle joint was unfeasible.

DISCUSSION

This study provided quantitative and qualitative data regarding the musculoskeletal anatomy of the long bones in live feral pigeons, potentially complementing clinical assessment of avian orthopedic patients. Each ROI was analyzed using both the short and long axes to get comprehensive data regarding total bone thickness, cortical thickness, and the evaluated tissue structure. Several limitations should be considered when interpreting the results of the statistical analysis. The relatively small sample size, particularly for the clavicle thickness (n = 17), limited the precision of the correlation estimates. Additionally, the conversion formula for the overall long bone thickness lacks validation in an independent cohort, which would be necessary to confirm its generalizability and clinical applicability across

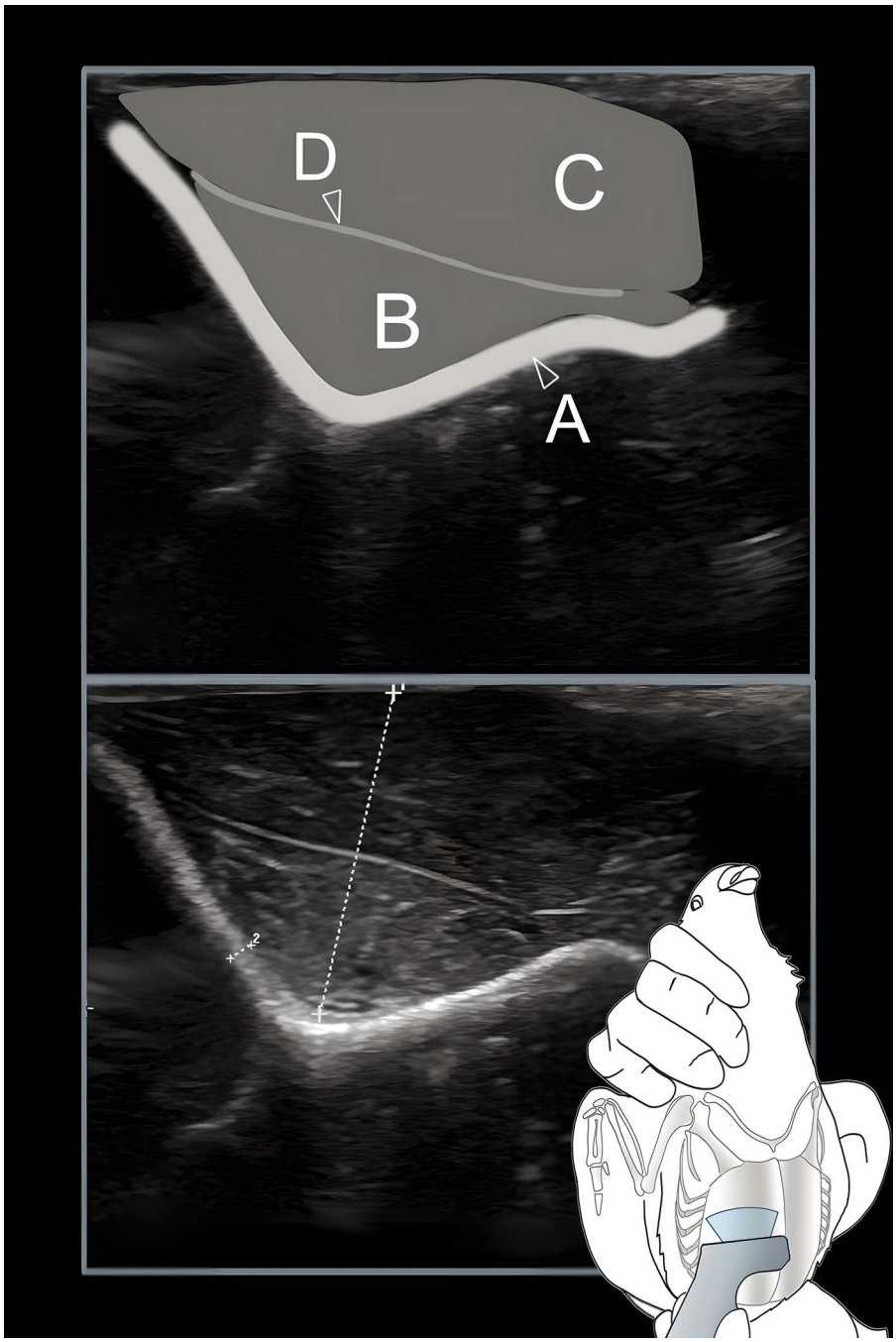

Figure 2. Normal B-mode ultrasound examination of the pectoral region in a feral pigeon (*Columba livia* f. dom.) (superimposed image of bird). The bone surface of the sternum body (*corpus sterni*) and keel (*carina sterni*) (A) could be observed as a hyperechogenic line. Deep pectoral muscle (*musculus pectoralis profundus*) (B) and superficial pectoral muscle (*m. pectoralis superficialis*) (C) could be defined through the intermuscular septum (D) appearing here as a narrow hyperechogenic line.

different populations and measurement settings. Although we found a statistically significant correlation between US and radiographic measurements for long bone thickness, the Lin CCC (CCC = 0.655) fell below the threshold of 0.9 considered indicative of moderately good agreement.[25] This suggests that further methodological refinement is necessary to improve measurement concordance between these techniques. However, future investigations should determine whether the current level of US accuracy may still provide clinical utility for specific applications, such as identifying animals with severely reduced long bone thickness when evaluating the feasibility of osteosynthesis procedures. Regarding the qualitative findings of the

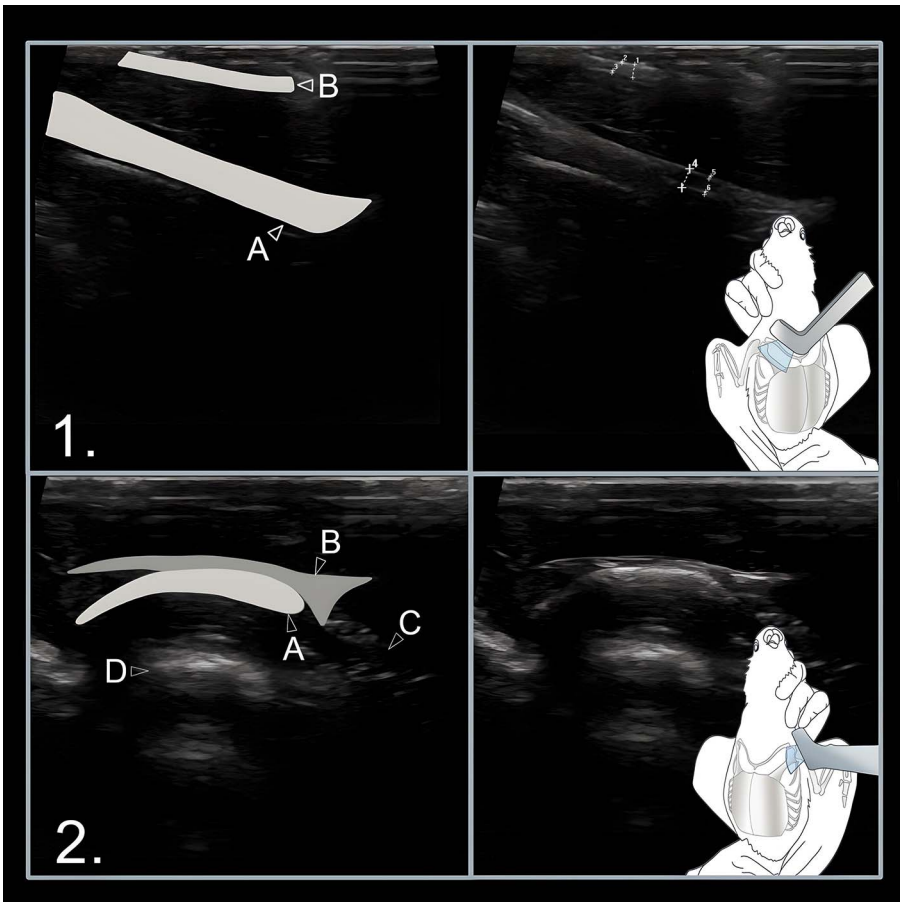

Figure 3. Normal B-mode ultrasound examination of the shoulder region in a feral pigeon (*Columba livia* f. dom.) showing coracoid (*os coracoideum*) (1A) and clavicle (*clavicula*) (1B). Both sides of the cortex and the medullary cavity can be observed. The shoulder joint's examination (2) allowed the displaying of the humeral head (A) and *lig. acrocoracohumeralis* (B) attending to the *m. supracoracoideus* (C). The reverberation effect ventrally from the humerus head surface can be observed as an irregular hyperechoic image (D). The ultrasound probe is placed in a sagittal position upon the clavicle.

study, the efficiency of using a high-frequency transducer for the small anatomical structures, described by several authors, was also confirmed in our study.[16,17,26,27] The limited assessment of bone structure in dogs and cats was a result of the reflection of US beams by dense bone structures and the acoustic shadowing that was cast.[19] However, the evaluation possibility of the assessed data was reported.[19] Our study produced comparable results, as imaging of the structures was frequently constrained by ultrasonic artifacts; nevertheless, accurate measurements were achievable in indicated ROIs. Due to the smaller size of our patients, a complete cross-section view of the long bone periosteum could be observed in almost all birds. When analyzing the long bones in a short-axis perspective, the pneumatization of certain large long bones (eg, humerus, femur) must be considered. As a result, the periosteal visualization may be restricted by the reverberation effect. It is important to consider the anatomical characteristics of various avian species in relation to the pneumatization of the peripheral bones. The presence of bone marrow in the femur has been observed in numerous *Charadriiformes* and many *Psittaciformes* species.[28] The pneumatization of the tibia in numerous raptors and of the radius in certain species must also be considered. Consequently, both the size of the bird and its structure may restrict the visualization due to the pneumatization of the bones. Gonzalez et al[14] report similar data in their research on the US evaluation of the long bones in cadavers of several species of *Accipitriformes* and *Strigiformes* birds; long bone thickness was also assessed. Thus, the data in our study indicates that US can possibly be employed to diagnose lesions or other pathological conditions of bone structures because it enables targeted examination. Nonetheless, the size of the avian patient and the ROI must be considered because the quality of the assessment may be constrained by reverberation

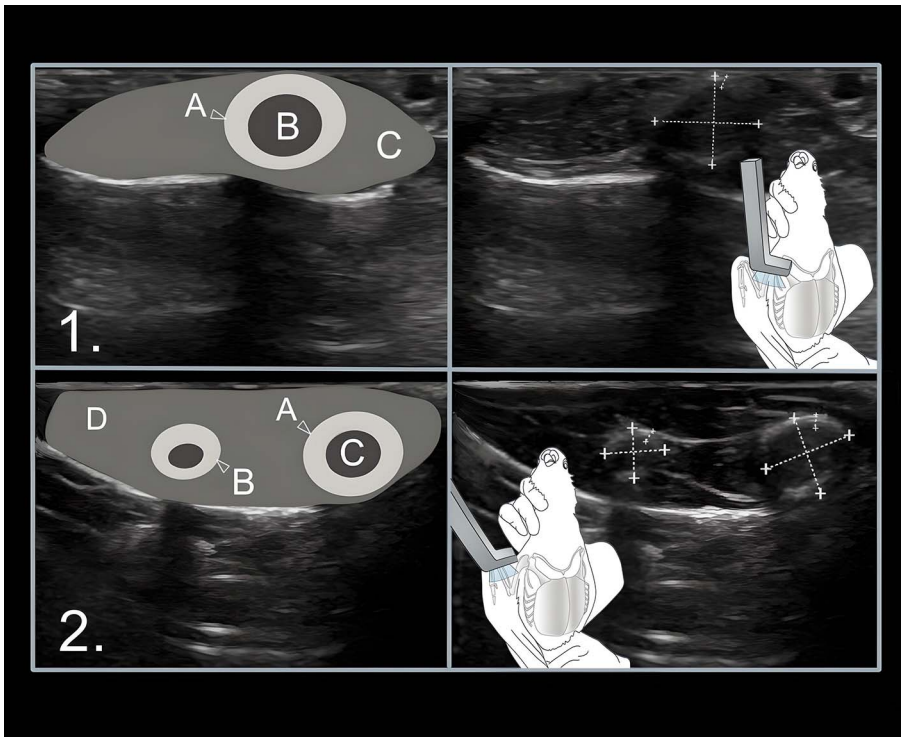

Figure 4. Normal B-mode ultrasound examination of the wing in a feral pigeon (*Columba livia* f. dom.) showing a cross-section of the humerus (1). The bone cortex (1A), intramedullary cavity (1B), and surrounding soft tissues of the humerus (1C) could be observed. The examination of the antebrachium showed the cross-section of the ulna (2A) and radius (2B) bones cortices, ulnar intramedullary cavity (2C), and surrounding soft tissues (2D). An ultrasound probe was placed transversally in the middle part of the humerus and forearm.

effects (in instances of pneumatized bones) or by insufficient thickness of the adjacent soft tissue or bone. Chew et al[17] and Lew et al[29] describe the assessment of tendon integrity as one of the best applications of the musculoskeletal US in human medicine. Tendons had the appearance of parallel, fibrillar lines overlying the bony surface in the longitudinal US. In our study, the ligamentous apparatus and the bursal cavity of the shoulder joint could be displayed in all birds. Avian skeletal muscles contain a lower proportion of connective and fatty tissue than mammalian muscles; however, the muscle fiber density of birds is generally higher.[30] According to the qualitative assessment reported in our study, the avian echostructure of soft tissues was like that of mammals. Similarly, the intermuscular fasciae were visible, allowing for the identification of specific muscles and muscle groups, which is critical when evaluating and considering motor function and muscle pathology. This should be considered when selecting a diagnostic imaging modality, depending on the area of interest and its accessibility. Despite this study, which predominantly focused on wild birds afflicted with musculoskeletal injuries or disorders, the authors believe that radiography remains the preferred diagnostic method for wild birds. This can be attributed to the greater accessibility and prevalence of radiographic units in wildlife rehabilitation centers and clinics as well as the fact that the primary diagnosis demands an overview examination of all locomotor apparatus structures. Moreover, the US transducer utilized in the study is not commonly employed in avian clinics, which is a limitation regarding the practical implementation of our results.

This study demonstrated that B-mode US can be used to examine the long bones, specific soft tissue components, and joints of live feral pigeons. The most accessible areas were the pectoral region, shoulder girdle, and shoulder joint. These anatomical sites are commonly affected in wild birds and are often difficult to diagnose using radiographic imaging. Sonographic imaging of the complete long bone section was possible in the birds used in this study (233–370 g). The large long bones (humerus and femur) of birds weighing less than 300 g allowed for sonographic imaging that provided the best diagnostic potential. A complete bone section could be observed in this case, including both sides of a hyperechoic cortex and the corresponding medullary cavity in the center. As a result, the sonographic examination provided clinical information on

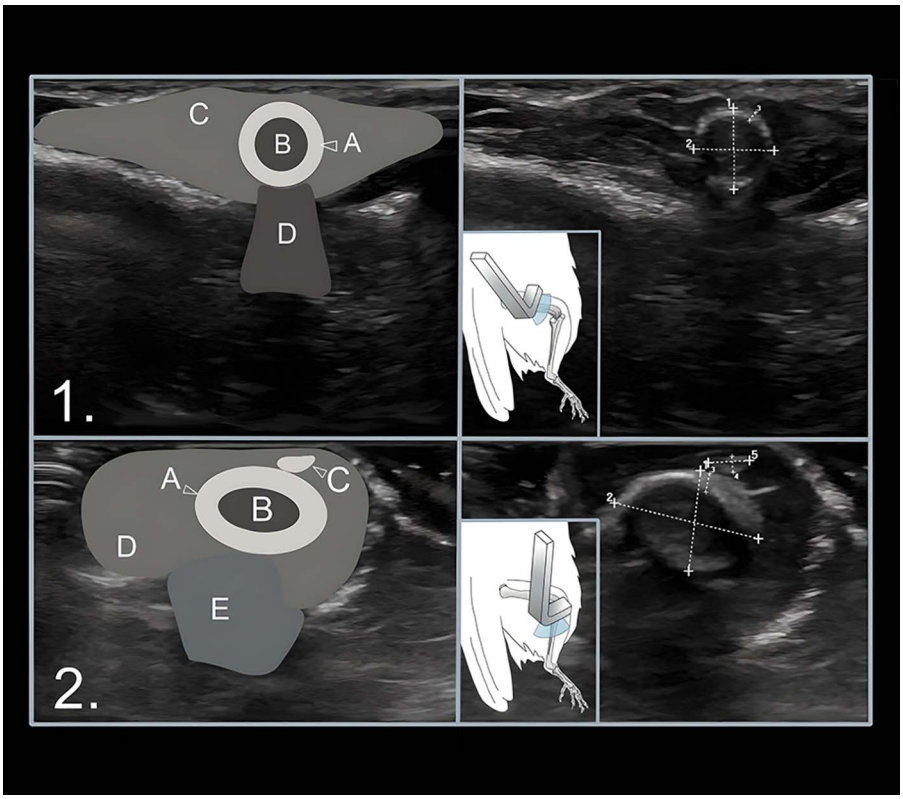

Figure 5. Normal B-mode ultrasound examination of the leg of a feral pigeon (*Columba livia* f. dom.) showing a cross-section of the femur (1). The bone cortex of the femur (1A), the medullary cavity (1B), and the surrounding soft tissues (1C) could be observed. The reverberation effect could be seen ventrally from the femoral bone (1D). The examination of the tibiotarsus (2) made it possible to visualize the cortices of the tibiotarsus (2A) and fibula (2C), the tibiotarsus intramedullary cavity (2B), and the surrounding soft tissues (2D). Note the reverberation produced and displayed below the tibiotarsal bone (2E). An ultrasound probe was placed transversally in the midlateral part of the femur and tibia.

the bone and soft tissue structures of the pectoral region, shoulder girdle, and shoulder joint. The shoulder, antebrachium, manus, and pelvic regions, including the stifle, provided less US imaging access but did not interfere with assessing anatomical structures. Thus, this study complements and enhances the diagnostic possibilities for avian orthopedic patients because US may be used as a complementary or, in some cases, alternative diagnostic imaging modality. The statistical analysis confirmed a significant concordance between the measurements for long bone thickness; however, the relatively small sample size, the observed level of correlation, and the lack of validation in an independent cohort limited the generalizability and clinical applicability of the findings. Future studies evaluating intact and damaged avian musculoskeletal structures across diverse populations and measuring contexts are needed to expand on the results of our investigation.

Acknowledgments: We thank the *Dres. Jutta & Georg Bruns Foundation* for the funding of this research study. We also wish to thank the Clinic for Birds and Reptiles staff team, University of Leipzig and the Institute of Medical Informatics, Statistic and Epidemiology, University of Leipzig for the technical support during the study.

REFERENCES

1. Calvo Carrasco D. Fracture management in avian species. *Veterinary Clin North Am Exot Anim Pract*. 2019;22:223–238.
2. McCabe KA, Rendle M, Harsch S, et al. Prognostic indicators of avian survival. *J Avian Med Surg*. 2020; 34:243–249.
3. King M, Giacinti J, Dubois S, et al. Using wildlife rehabilitation and postmortem data to identify key causes of morbidity and mortality impacting the health and welfare of free-living wild animals in Canada. *J Wildl Dis*. 2023;59:93–108.
4. Vergneau-Grosset C, Kapatkin AS, Paul-Murphy J, et al. Release rates and complications for birds of prey with antebrachial fractures at a veterinary teaching hospital. *J Avian Med Surg*. 2019;33:388–397.
5. Rhim H, Gahng J, Baek G, et al. Morbidity of rescued wild birds by admission causes in the Republic of Korea. *Animals*. 2024;14:2071.

6. Willette M, Rosenhagen N, Buhl G, et al. Interrupted lives: welfare considerations in wildlife rehabilitation. *Animals*. 2023;13:1836.
7. Scheelings TF. Coracoid fractures in wild birds: a comparison of surgical repair versus conservative treatment. *J Avian Med Surg*. 2014;28:304–308.
8. Azmanis PN, Wernick MB, Hatt JM. Avian luxations: occurrence, diagnosis and treatment. *Vet Q*. 2014;34:11–21.
9. Krautwald-Junghanns ME, Pees E, Reese S, et al. *Diagnostic Imaging of Exotic Pets*. Schlütersche Verlagsgesellschaft; 2011.
10. Gumpenberger M, Kolm G. Ultrasonographic and computed tomographic examinations of the avian eye: physiologic appearance, pathologic findings, and comparative biometric measurement. *Vet Radiol Ultrasound*. 2006; 47:492–502.
11. Vilaplana Grosso F. Orthopedic diagnostic imaging in exotic pets. *Veterinary Clin North Am Exot Anim Pract*. 2019;22:149–173.
12. Williams J. Orthopedic radiography in exotic animal practice. *Veterinary Clin North Am Exot Anim Pract*. 2002; 5:1–22.
13. Visser M, Hespel AM, de Swarte M, et al. Use of a caudoventral-craniodorsal oblique radiographic view made at 45° to the frontal plane to evaluate the pectoral girdle in raptors. *J Am Vet Med Assoc*. 2015;247:1037–1041.
14. González CAG, Lopes CTA, Teixeira PPM, et al. B-mode ultrasonographic evaluation of long bones in Falconiformes and Strigiformes birds. *Avian Pathol*. 2018; 47:625–629.
15. Meikle B, Stephan CN. B-mode ultrasound measurement of facial soft tissue thickness for craniofacial identification: a standardized approach. *J Forensic Sci*. 2020;65: 939–947.
16. Frank I, Duerr F, Zanghi B, et al. Diagnostic ultrasound detection of changes in femoral muscle mass recovery after tibial plateau levelling osteotomy in dogs. *Vet Comp Orthop Traumatol*. 2019;32:394–400.
17. Chew K, Stevens KJ, Wang TG, et al. Introduction to diagnostic musculoskeletal ultrasound: part 2: examination of the lower limb. *Am J Phys Med Rehabil*. 2008;87:238–248.
18. Mah JK, van Alfen N. Neuromuscular ultrasound: clinical applications and diagnostic values. *Can J Neurol Sci*. 2018; 45:605–619.
19. Kramer M, Gerwing M, Hach V, et al. Sonography of the musculoskeletal system in dogs and cats. *Vet Radiol Ultrasound*. 1997;38:139–149.
20. Tabozzi SA, Stancari G, Zucca E, et al. Variation of skeletal muscle ultrasound imaging intensity in horses after treadmill exercise: a proof of concept for glycogen content estimation. *BMC Vet Res*. 2021;17:121.
21. Zaw AM, Shangguan R, Yao Y, et al. Vascular imaging in small animals using clinical ultrasound scanners. *Methods Mol Biol*. 2022;2375:191–201.
22. Chitty J, Lierz M. *BSAVA Manual of Raptors, Pigeons and Passerine Birds*. BSAVA Library; 2008.
23. Kaleta EF, Krautwald-Junghanns ME. *Kompendium der Ziervogelkrankheiten*. Schlütersche Verlagsgesellschaft; 2011.
24. Signorell A, Aho K, Alfons A, et al. DescTools: Tools for Descriptive Statistics. R package version 0.99.60. Vienna, Austria: R Foundation for Statistical Computing; 2024. Available from: https://CRAN.R-project.org/package=DescTools. Accessed January 10, 2026.
25. Akoglu H. User's guide to correlation coefficients. *Turk J Emerg Med*. 2018;18:91–93.
26. Jiménez-Díaz F, Jimena I, Luque E, et al. Experimental muscle injury: correlation between ultrasound and histological findings. *Muscle Nerve*. 2012;45:705–712.
27. Naredo E, Medina JP, Pérez-Baos S, et al. Validation of musculoskeletal ultrasound in the assessment of experimental gut synovitis. *Ultrasound Med Biol*. 2018; 44:1516–1524.
28. Cubo J, Casinos A. Incidence and mechanical significance of pneumatization in the long bones of birds. *Zool J Linn Soc*. 2000;130:499–510.
29. Lew HL, Chen CPC, Wang TG, et al. Introduction to musculoskeletal diagnostic ultrasound: examination of the upper limb. *Am J Phys Med Rehabil*. 2007;86:310–321.
30. King AS, McLelland J. *Form and Function in Birds*. Academic Press; 1985.